Signature of the two-dimensional phonon dispersion in graphene probed by double-resonant Raman scattering

Patrick May,[1,*] Michele Lazzeri,[2] Pedro Venezuela,[3] Felix Herziger,[1] Gordon Callsen,[1] Juan S. Reparaz,[1,†] Axel Hoffmann,[1] Francesco Mauri,[2] and Janina Maultzsch[1]

[1]*Institut für Festkörperphysik, Technische Universität Berlin, Hardenbergstraße 36, D-10623 Berlin, Germany*
[2]*IMPMC, Université Pierre et Marie Curie, CNRS, 4 place Jussieu, F-75252 Paris, France*
[3]*Instituto de Física da Universidade Federal Fluminense, Campus da Praia Vermelha, Niterói, RJ, Brazil*

(Received 20 September 2012; revised manuscript received 9 January 2013; published 4 February 2013)

The contributions of the two-dimensional phonon dispersion to the double-resonant Raman scattering process in graphene is determined from the line shape of the two-phonon combination mode around 2450 cm^{-1}. This mode is usually referred to as G^* or $D + D''$. By combining Raman experiments with excitation energies up to 2.8 eV and a full two-dimensional calculation of the double-resonant Raman process based on fourth-order perturbation, we can describe in detail the composition of this two-phonon mode and explain the asymmetry on the high-frequency side. The asymmetry directly reflects phonon contributions with wave vectors away from the high-symmetry lines in the Brillouin zone. The main peak of this mode originates from the **KΓ** high-symmetry line highlighting and supporting two important findings: first, the existence of so-called *inner* processes and, second, the dominant contribution along the high-symmetry line.

DOI: 10.1103/PhysRevB.87.075402 PACS number(s): 78.67.Wj, 81.05.ue, 78.30.Na, 63.22.Rc

The electrical and mechanical properties of graphene are very sensitive to external perturbations. For example by introducing additional layers of graphene a tunable band gap in both bilayer[1] and trilayer graphene[2–4] can be opened. Further, the single- and double-resonant scattering paths can be influenced by electrostatic doping.[5] The changes of the electrical and mechanical properties can be probed by Raman scattering:[6,7] It can be applied to monitor strain and also derive the crystallographic orientation of two-dimensional graphene;[8–12] it probes structural defects,[13–16] stacking order,[17–19] edge orientation,[20] and functionalization;[21] and in one-dimensional carbon nanotubes diameter[22] and many-body effects[23] can be accessed.

Especially double-resonant Raman scattering[24] attracted a great deal of attention. A recent fundamental question in the literature concerns dominant scattering paths of electrons and phonons within the two-dimensional Brillouin zone. Here, recent discussions aimed at the understanding whether either so-called *inner* or *outer* processes give rise to the $2D$ (sometimes named G') peak in the Raman spectrum.[10,11,25–29]

Besides the $2D$ mode, several other double-resonant Raman modes appear in the spectrum of graphene. The origin of some of them is still under discussion as in the case of an asymmetric peak around 2450 cm^{-1}. In the literature this mode is usually named the $D + D''$[27,30,31] or G^*[32] mode. $D + D''$ refers to a two-phonon process involving the contribution of a transverse optical (TO) and longitudinal acoustic (LA) phonon, where following Ref. 27 TO $\rightarrow$ D and LA $\rightarrow$ D''. This combination was suggested in Refs. 30–32 as the origin of the $\approx$2450 cm^{-1} mode. Reference 33 reported a nondispersive behavior attributed to the overtone of the LO phonon at the **K** point. However, these publications did not explain the asymmetric line shape. Recently Ref. 34 suggested an interpretation of the asymmetry. The asymmetric tail was explained as due to a double-resonant process involving two phonons of the D phonon branch from the **K** point. This contribution, however, should cancel by destructive interference.[35]

In this article we unravel the origin of the two-phonon $D + D''$ peak and its asymmetric line shape by combining experimental data of single-layer graphene with a full two-dimensional calculation of the double-resonant Raman process based on fourth-order perturbation theory. We show that the main peak originates from phonons along the **KΓ** high-symmetry line and that the asymmetry is due to phonons from the two-dimensional Brillouin zone. The analysis of the asymmetric line shape in experiment provides a direct probe of the two-dimensional phonon dispersion. We further show how the $D + D''$ peak evolves with the number of graphene layers.

We investigated mechanically exfoliated single-layer graphene, which was deposited on SiO_2. The layer thickness was determined first by optical contrast and then confirmed by measuring the $2D$ and N mode.[25,36] Confocal μ-Raman spectroscopy was performed in backscattering geometry under ambient conditions. The setup provides a spectral resolution around 1 cm^{-1}. The Raman spectra were simulated using the method described in Ref. 27, with the same computational details. In particular, the Raman cross section is obtained from the fourth-order perturbative approach (the same approximation which is inherent to the double-resonance approach of Ref. 24); we consider all possible transitions among the π/π^* electronic bands in the two-dimensional graphene Brillouin zone, including the scattering with all possible phonons, in the two-dimensional Brillouin zone.

Figure 1 shows the measured and calculated Raman spectra of single-layer graphene for the $D + D''$ peak at three different excitation energies. We observe a main contribution and an asymmetric tail towards higher frequencies. Both the peak positions and the asymmetric line shape are correctly reproduced by the calculation (see below). In order to quantify the width of the high-frequency tail, measurements were fitted with two Lorentzians and a linear background. The inset of Fig. 1 reports the evolution of the two Lorentzian maxima as a function of the excitation energy. In contrast to Ref. 34, we

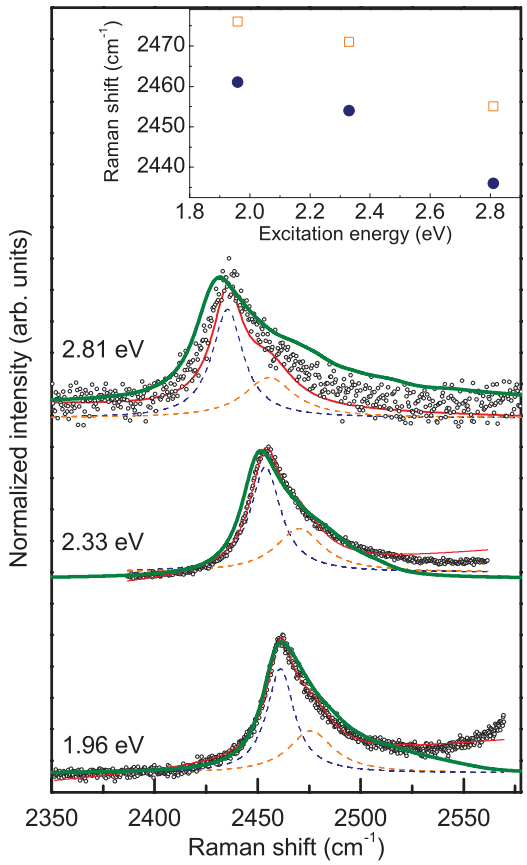

FIG. 1. (Color online) Raman spectra of single-layer graphene on SiO_2 for three different excitation energies (open circles) fitted each with two Lorentzian profiles (dashed lines). The solid red line is the fit of the two Lorentzian profiles. The solid thick line (green) is obtained from calculations. The inset depicts the shift of the Lorentzians versus the excitation energy from the fitted experimental data.

observe a clear dispersive behavior of the two contributions. This may be attributed to the extended range of excitation energies in our experiment: The $D + D''$ peak exhibits only very small shift rates around $\approx$2 eV (i.e., in the excitation energy range in Ref. 34), as can be seen in the inset of Fig. 1.

In order to understand the behavior of the $D + D''$ peak, we first remember that two-phonon Raman scattering can be schematized as the result of four "virtual" transitions: absorption of a quantum of light (and creation of an electron-hole pair), scattering of an electronic state with a phonon with wave vector $\mathbf{q}$, scattering of an electronic state with a phonon with wave vector $-\mathbf{q}$, and electron-hole recombination and emission of a quantum of light. The relevant electronic states in the process are the π and π^* bands with energy $\epsilon^{\pi}_{\mathbf{k}}$, $\epsilon^{\pi*}_{\mathbf{k}}$ ($\mathbf{k}$ is the wave vector). The wave vectors $\mathbf{k}$ of the electronic states that are excited by a laser with energy ϵ_L (and those that are involved in the emission of a quantum of light $\epsilon_L - \epsilon_{ph}$) form a triangularly distorted closed line, as the isoenergy contour surrounding the high-symmetry $\mathbf{K}$ (and $\mathbf{K}'$) point in Fig. 2(a). Following the double-resonance (DR) idea,[24] the electronic states of these isoenergy contours provide the most important contribution to the Raman scattering process. The phonons which dominate the scattering have a wave vector $\mathbf{q}_n$ such that by translating the first isoenergy contour by $\mathbf{q}_n$, it becomes tangent to the second one [Fig. 2(a)]. Indeed, these processes are associated with high density of resonant transitions and are enhanced by interference effects.[27] The ensemble of the nesting vectors $\mathbf{q}_n$ represents the momenta of the dominant phonon contributions and determines the two closed lines surrounding $\mathbf{K}$ and $\mathbf{K}'$ in Fig. 2(b). The angle θ is defined as that $\theta = 0^\circ$ corresponds to the $\mathbf{K\Gamma}$ high-symmetry line (*inner* process phonons) and $\theta = \pm 60^\circ$ corresponds to the $\mathbf{KM}$ one (*outer* process phonons).

Figure 2(c) depicts the energies of the three highest phonon branches of graphene (labeled 4, 5, and 6) calculated along the DR profile [the nesting vector $\mathbf{q}_n$ line of Fig. 2(b)]. These three phonon branches are responsible for the $D, 2D$, and D'' Raman peaks. The D'' peak is known as a weak defect-induced one-phonon process and should be observed at $\sim$1100 cm^{-1}.[27] The phonons responsible for the D peak have an almost constant frequency of $\sim$1350 cm^{-1} at a fixed excitation energy and correspond to the 5th phonon branch along the $\mathbf{K\Gamma}$ ($|\theta| \lesssim 30^\circ$) high-symmetry line and to the 6th phonon branch along the $\mathbf{KM}$ direction ($60^\circ \gtrsim |\theta| \gtrsim 30^\circ$). The 4th phonon branch shows a strong angular dispersion along the DR profile, going from $\sim$1100 cm^{-1} along the $\mathbf{K\Gamma}$ direction to 1240 cm^{-1} along the $\mathbf{KM}$ direction. Notice that, in the literature, the branch associated with the D peak is usually labeled as TO (it is actually TO only in the neighborhood of $\mathbf{\Gamma}$) and it is affected by a Kohn anomaly near $\mathbf{K}$.[37] The TO branch [which is the 6th branch in the vicinity of $\mathbf{K}$ but it is the 5th one sufficiently far from $\mathbf{K}$; see Fig. 2(d)] appears as a continuous line only along the $\mathbf{\Gamma KM}$ directions [Fig. 2(d)]. In other points of the Brillouin zone the 5th and 6th branches form an avoided crossing[38] [Fig. 2(c)].

Having the two-dimensional phonon contributions in mind, we can now analyze the theoretical results. The calculated intensity of a Raman peak can be decomposed into the different contributions $\mathcal{I}_{\mathbf{q}}$ associated with phonons with different wave vectors $\mathbf{q}$, following the procedure described in Ref. 27. Figure 3(d) shows the $\mathcal{I}_{\mathbf{q}}$ decomposition associated to the $D + D''$ peak and depicts only the intensity associated with the phonon transitions involving the "4 + 5" and "4 + 6" branches. According to calculations, other contributions (e.g., that from the "6 + 6" branches) are negligible at 2450 cm^{-1}. The decomposition of the intensity $\mathcal{I}_{\mathbf{q}}$ is significantly different from zero in a region forming two relatively narrow lines surrounding $\mathbf{K}$ and $\mathbf{K}'$ (as expected from DR). Figure 3 also reports the phonon branches contributing to the $D + D''$ mode as function of the angle θ [as defined in Fig. 2(a)]. Figures 3(a)–3(c) can be read both vertically and horizontally. Figures 3(a) and 3(b) connect the frequency horizontally, while Figs. 3(a) and 3(c) connect the angle θ vertically. Both the frequency and the angle θ are related to the intensity. Figure 3(a) shows (as dots) the frequency associated with the maxima of the $\mathcal{I}_{\mathbf{q}}$ of Fig. 3(d). Figure 3(d) is a two-dimensional contour plot of the contributing phonons. Figure 3(a) also reports the frequency of the branches "4 + 5" and "4 + 6" calculated along the DR profile of Fig. 2(b). The theoretical Raman shift for a given angle θ [dots in Fig. 3(a)] nicely coincides with the "4 + 6" line for $|\theta| \gtrsim 30^\circ$ and with the "4 + 5" line for $|\theta| < 30^\circ$. This result can be interpreted by looking at Fig. 2(c): The DR Raman frequency coincides with the sum of the frequency of the 4th branch and that of the

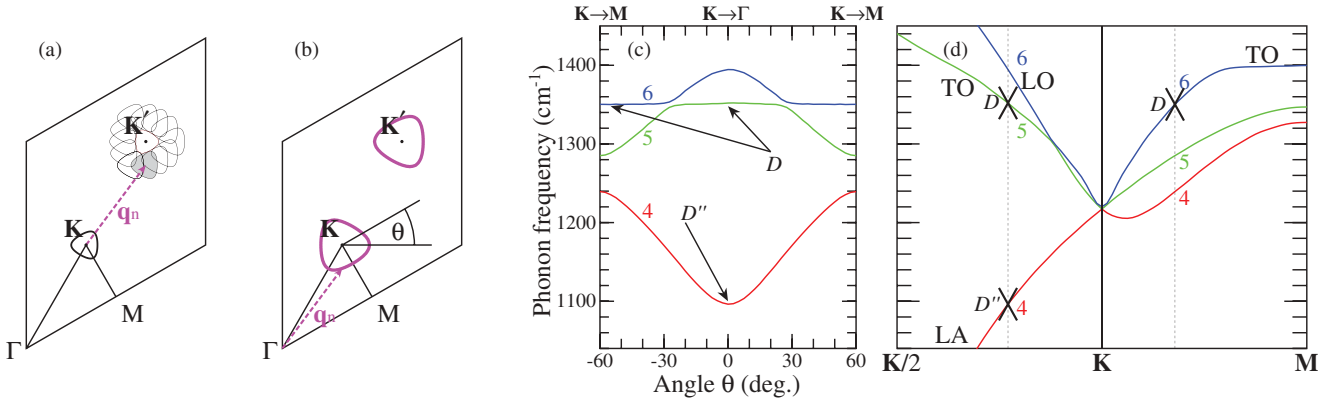

FIG. 2. (Color online) (a) The rhombus is the graphene Brillouin zone. The triangularly distorted contour around **K** is obtained from $\epsilon^{\pi^*}_{\mathbf{k}} - \epsilon^{\pi}_{\mathbf{k}} = 2.33$ eV and represents the electronic states near **K** that are excited by a laser with energy $\epsilon_L = 2.33$ eV. The contour around $\mathbf{K}' = 2\mathbf{K}$ is obtained from $\epsilon^{\pi^*}_{\mathbf{k}} - \epsilon^{\pi}_{\mathbf{k}} = 2.03$ eV and represents the electronic states near $\mathbf{K}'$ that are deexcited by the emission of a quantum of light with energy $\epsilon_L - \hbar\omega_{ph}$, with $\omega_{ph} = 2450$ cm^{-1} (the energy of the $D + D''$ line for $\epsilon_L = 2.33$ eV). $\mathbf{q}_n$ is one of the vectors such that the contour near **K** translated by $\mathbf{q}_n$ is tangent to the contour near $\mathbf{K}'$. (b) The contours around **K** and $\mathbf{K}'$ are the ensemble of the $\mathbf{q}_n$ vectors. These are the wave vectors of the phonons mostly involved in the double resonance. (c) Frequency of the three highest phonon branches (labeled 4, 5, and 6) calculated along the contours shown in panel (b) and plotted as a function of the angle θ defined in panel (b). $\theta = 0°$ corresponds to the **KΓ** high-symmetry line and $\theta = \pm 60°$ corresponds to the **KM** one. (d) Dispersion of the three highest phonon branches along the high-symmetry line **ΓKM**. The vertical dotted lines identify the phonons selected by the DR condition of panel (b). The crosses represent the phonons mostly responsible for the D and D'' Raman peaks at $\epsilon_L = 2.33$ eV.

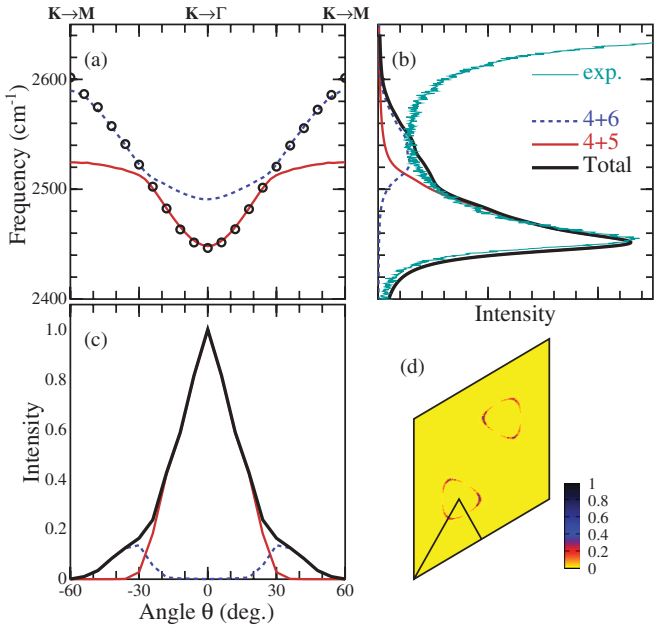

FIG. 3. (Color online) (a) Lines are the sum of the phonon frequencies of the branch couples "4 + 5" and "4 + 6" calculated along the $\mathbf{q}_n$ line of Fig. 2(b). The frequencies are plotted as a function of the angle θ, as in Figs. 2(b) and 2(c). Dots show the theoretical Raman shift of the $D + D''$ peak as a function of the angle θ. (b) Measured (exp.) and calculated (Total) Raman intensity of the $D + D''$ peak at $\epsilon_L = 2.33$ eV. Calculations are decomposed into "4 + 5" and "4 + 6" phonon branch contributions. (c) Theoretical Raman intensity of the $D + D''$ peak as a function of the θ and decomposed into the "4 + 5" and "4 + 6" contributions. (d) Theoretical Raman intensity $\mathcal{I}_{\mathbf{q}}$ of the $D + D''$ mode (see the text); the rhombus has the same meaning as in Fig. 2.

branch associated with the D peak (which is the 6th branch for $|\theta| \gtrsim 30°$ and the 5th for $|\theta| < 30°$).

Figure 3(b) compares the measured Raman $D + D''$ intensity with the calculated one for $\epsilon_L = 2.33$ eV. Figure 3(c) reports the intensity of the branches "4 + 5" and "4 + 6" and the total as a function of the angle θ. It further shows that the dominant contribution comes from $\theta \approx 0°$, which is along the **KM** high-symmetry direction. In the literature, these are usually called *inner* phonon processes. Unlike for the $2D$ mode as shown in Ref. 27, the $D + D''$ mode has no contribution from *outer* processes due to zero electron-phonon coupling elements.

The emerging picture can be resumed as follows. The $D + D''$ peak is the combination of a phonon associated with the branch responsible for the D (5th or 6th phonon branch depending on the direction in the Brillouin zone) peak and a second phonon associated with the 4th phonon branch. The momenta of the relevant phonons are selected by the DR conditions and identify a closed line surrounding the high symmetry **K** point [Fig. 2(b)]. Along this line the frequency of the D phonons is almost constant, while that of the 4th branch undergoes a strong dispersion. The most intense processes take place along the **KΓ** direction (*inner* processes), where the frequency of the 4th branch has a minimum. Other processes along different directions, where the 4th branch has a higher frequency, are possible but are less intense and provide the observed high-frequency tail and its decreasing intensity due to less dominant electron-phonon and electron-photon coupling entering in the Raman cross section. It is important to notice that the dots of Fig. 3(a) are obtained from our best calculations (which are done without making any assumption concerning the validity of the DR). On the contrary, the lines of Fig. 3(a) are obtained from the simplified scheme of Fig. 2 (which is

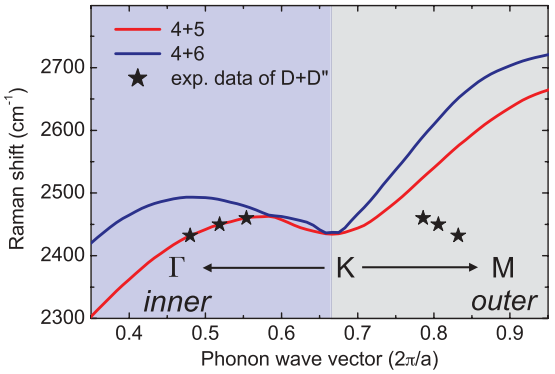

FIG. 4. (Color online) Sum of the 4th and 5th and the 4th and 6th phonon branch along the **ΓKM** high-symmetry direction as a function of the phonon wave vector. Points are measured frequencies of single-layer graphene and assigned to the corresponding phonon wave vector of both *inner* and *outer* processes. $2\pi/a$ corresponds to the distance (**ΓKM**), where a is the in-plane lattice constant of graphene. Note that the sum of the 4th and 6th phonon branch along the high-symmetry line does not contribute to the Raman intensity; see Fig. 3(c) at $\Theta = 0$.

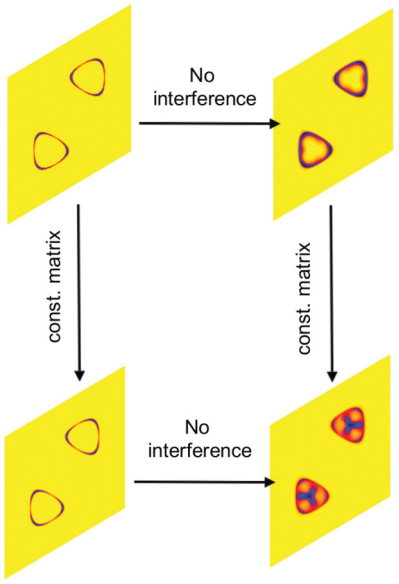

FIG. 5. (Color online) $\mathcal{I}_{\mathbf{q}}$ decomposition of the intensity of the Raman $2D$ peak for $\epsilon_L = 2.33$ eV. The rhombus has the same meaning as in Fig. 2. The four panels result from calculations done with different kinds of approximations. The upper left panel is our best calculation [same calculation as in Fig. 3(d)]. The panels on the right are obtained by neglecting interference effects and the bottom panels are obtained by considering constant electron-phonon scattering matrix elements.

based on the DR idea). The nice agreement between the two approaches implies that the DR captures the relevant physics of the problem.

Now, in order to show how the wave vectors of the excited phonons change as a function of the excitation laser, we consider a one-dimensional approach along the high-symmetry line (**ΓKM**). Figure 4 shows along the ΓKM direction the sum of the 4th and the 5th and the sum of the 4th and the 6th phonon branch. The frequency of the main contribution (blue dashed line in Fig. 1) is plotted versus the calculated phonon wave vector.

The phonon wave vector is calculated from the double-resonant processes that satisfy the double-resonant condition in one dimension. We observe two important results. First, the experimental data only match the phonons from a certain direction in the Brillouin zone, namely the **KΓ** direction. This involves electronic excitations between the **KM** direction, which in the literature is called an *inner* process. Second, according to the evolution of the phonon dispersion in Fig. 4, the dispersion around ≈0.53 to 0.60 ($2\pi/a$), which corresponds to excitations around 2.4 to 1.9 eV, is small. This might explain the almost constant Raman frequency found in Ref. 34 for a small excitation energy range.

Finally, it has been argued in Ref. 34 that the origin of the high-frequency tail of the $D + D''$ peak is due to two phonons, which are responsible for the D peak at the **K** point. We therefore calculate the Raman intensity of the $2D$ peak. According to our calculations the Raman signal associated with this phonon is negligible because of two reasons: (i) quantum interference and (ii) electron-phonon scattering selection rules. The role of quantum interference is understood by considering that the Raman signal results from the sum of scattering amplitudes associated with different processes. These are complex numbers which can interfere in a constructive or in a destructive way (see Ref. 35 and Sec. III E 1 of Ref. 27). The wave vectors of the phonons providing a Raman signal belong to a narrow region surrounding the **K** point [Fig. 3(d)]. This region is so narrow not only because of the DR scheme presently described in relation to Fig. 2, but also because of the role played by the quantum interference.[35] In the absence of quantum interference, one could excite phonons beyond this region and, possibly, excite also the phonons with $\mathbf{q} = \mathbf{K}$ (see Ref. 35 and Appendix D of Ref. 27). On the other hand, as already pointed out in Ref. 24, the relevant electron-phonon coupling matrix elements among the π/π^* electronic bands and the phonon with $\mathbf{q} = \mathbf{K}$ are zero (see also note 24 of Ref. 37) and the phonon is not Raman active.

To visualize these above mentioned concepts, in Fig. 5 we report the $\mathcal{I}_{\mathbf{q}}$ decomposition of the $2D$ peak calculated with different levels of approximations: (i) We do not consider quantum interference effects (the Raman signal is obtained by summing the modulus of the scattering amplitudes, as in Sec. III E 1 of Ref. 27) and (ii) we fix to a constant the electron-phonon scattering matrix elements (we neglect the dependence on the electron and phonon wave vectors, $\mathbf{k}$ and $\mathbf{q}$, in the numerators of the scattering amplitudes, K in Ref. 27). From Fig. 5, we see that in the absence of quantum interference, the phonons providing a Raman signal belong to broader region. However, the phonons with $\mathbf{q} = \mathbf{K}$ are not yet active ($\mathcal{I}_{\mathbf{q}} \sim 0$ for $\mathbf{q} = \mathbf{K}$). On the other hand, when we also consider the electron-phonon matrix elements as constants, the $\mathbf{q} = \mathbf{K}$ phonon becomes Raman active ($\mathcal{I}_{\mathbf{q}} \neq 0$ for $\mathbf{q} = \mathbf{K}$). Therefore both the electron-phonon matrix elements and the interference effects suppress phonons with $\mathbf{q} = \mathbf{K}$.

Finally, we will show how the $D + D''$ peak evolves with the number of layers. The electronic properties of graphene depend on the number of layers and the interactions between them. This introduces additional scattering processes in the

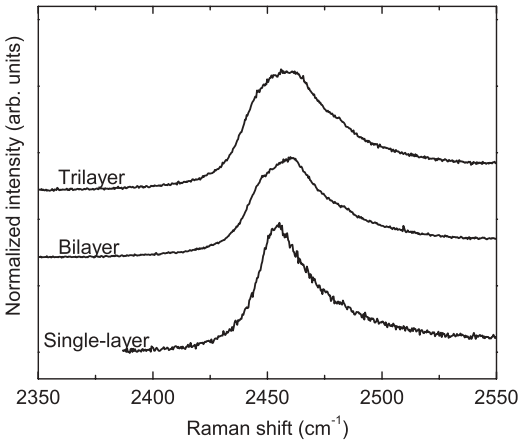

FIG. 6. Experimental $D + D''$ spectrum for single-layer, bilayer, and trilayer graphene excited at 2.33 eV. Each spectrum is normalized and vertically offset for better graphical representation.

double-resonant scattering. Similar to the $2D$ mode, the $D + D''$ peak exhibits additional contributions for increasing layer number. This is shown in Fig. 6 for single-layer, bilayer, and trilayer graphene at 2.33 eV excitation energy. For single-layer graphene, the $D + D''$ peak exhibits a main contribution and an asymmetric line shape towards higher frequencies as discussed above in detail. For bi- and trilayer graphene additional contributions appear. This can be understood when considering the main contribution which stems from the high-symmetry line along the **KΓ** direction (*inner* process). Due to two and three valence and conduction bands for bi- and trilayer, respectively, additional scattering processes occur leading to slightly different phonon wave vectors and consequently changes in the electronic structure are also captured in the $D + D''$ peak. Note that these changes in the line shape depend on the excitation energy, and the difference is vanishing at 1.96 eV. The vanishing is due to different phonon wave vectors **q** that result in the same phonon frequency in the vicinity of a zero slope of the 4th and 5th phonon branch at around 0.55 (2π/a) in Fig. 4. We expect an increasing separation for the main contribution when changing the excitation energy as a consequence of the increasing slope of the corresponding phonon branches.

In conclusion, we have revealed the origin of the double-resonant two-phonon $D + D''$ peak. The main contribution of this peak originates from so-called *inner* processes, i.e., phonons from the **KΓ** direction. The asymmetric line shape on the high-frequency side comes from additional, weaker contributions from phonon wave vectors with angles deviating up to 60 degrees from the **KΓ** line. The decrease of the intensity towards higher frequencies is a direct consequence of the electron-phonon and electron-photon matrix elements entering the Raman cross section in the double-resonant process. We believe that the insights into the scattering processes and the ability to probe directly the two-dimensional phonon dispersion with Raman scattering may provide useful analysis in the future, especially concerning effects of functionalization and defects. By combining measurements of the $2D$ and $D + D''$ mode it will be possible to extract modifications in the phonon structure of the D'' phonon branch, for instance under strain or functionalization. Further, depending on the excitation energy, this combination mode is useful for the determination of the number of layers in graphene, in addition to the $2D$ and N mode.

P.M. and J.M. acknowledge financial support from the DFG under Grant No. MA 4079/3-1 and from the European Research Council (ERC) Grant No. 259286. Part of the calculations were done at IDRIS, Project No. 096128.

*pmay@physik.tu-berlin.de
†Present address: Institut de Ciència de Materials de Barcelona-CSIC, Esfera UAB, 08193 Bellaterra, Spain.

[1] Y. Zhang, T.-T. Tang, C. Girit, Z. Hao, M. C. Martin, A. Zettl, M. F. Crommie, Y. R. Shen, and F. Wang, Nature (London) **459**, 820 (2009).
[2] C. H. Lui, Z. Li, K. F. Mak, E. Cappelluti, and T. F. Heinz, Nat. Phys. **7**, 944 (2011).
[3] W. Bao, L. Jing, J. Velasco, Y. Lee, G. Liu, D. Tran, B. Standley, M. Aykol, S. B. Cronin, D. Smirnov *et al.*, Nat. Phys. **7**, 948 (2011).
[4] L. Zhang, Y. Zhang, J. Camacho, M. Khodas, and I. Zaliznyak, Nat. Phys. **7**, 953 (2011).
[5] C.-F. Chen, C.-H. Park, B. W. Boudouris, J. Horng, B. Geng, C. Girit, A. Zettl, M. F. Crommie, R. A. Segalman, S. G. Louie *et al.*, Nature (London) **471**, 617 (2011).
[6] S. Reich, C. Thomsen, and J. Maultzsch, in *Carbon Nanotubes: Basic Concepts and Physical Properties* (Wiley-VCH, Berlin, 2004).
[7] A. Jorio, M. Dresselhaus, R. Saito, and G. F. Dresselhaus, *Raman Spectroscopy in Graphene Related Systems* (Wiley-VCH, Berlin, 2011).
[8] T. Mohiuddin, A. Lombardo, R. Nair, A. Bonetti, G. Savini, R. Jalil, N. Bonini, D. Basko, C. Galiotis, N. Marzari *et al.*, Phys. Rev. B **79**, 205433 (2009).
[9] M. Huang, H. Yan, C. Chen, D. Song, T. Heinz, and J. Hone, Proc. Natl. Acad. Sci. **106**, 7304 (2009).
[10] M. Huang, H. Yan, T. F. Heinz, and J. Hone, Nano Lett. **10**, 4074 (2010).
[11] O. Frank, M. Mohr, J. Maultzsch, C. Thomsen, I. Riaz, R. Jalil, K. Novoselov, G. Tsoukleri, J. Parthenios, and K. Papagelis, ACS Nano **5**, 2231 (2011).
[12] J. Zabel, R. R. Nair, A. Ott, T. Georgiou, A. K. Geim, K. S. Noyoselov, and C. Casiraghi, Nano Lett. **12**, 617 (2012).
[13] F. Banhart, J. Kotakoski, and A. Krasheninnikov, ACS Nano **5**, 26 (2011).
[14] A. Eckmann, A. Felten, A. Mishchenko, L. Britnell, R. Krupke, K. Novoselov, and C. Casiraghi, Nano Lett. **12**, 3925 (2012).
[15] E. H. Martins Ferreira, M. V. O. Moutinho, F. Stavale, M. M. Lucchese, R. B. Capaz, C. A. Achete, and A. Jorio, Phys. Rev. B **82**, 125429 (2010).
[16] L. G. Cançado, A. Jorio, E. H. M. Ferreira, F. Stavale, C. A. Achete, R. B. Capaz, M. V. O. Moutinho, A. Lombardo, T. S. Kulmala, and A. C. Ferrari, Nano Lett. **11**, 3190 (2011).

[17]C. H. Lui, Z. Li, Z. Chen, P. V. Klimov, L. E. Brus, and T. F. Heinz, Nano Lett. **11**, 164 (2011).
[18]R. Rao, R. Podila, R. Tsuchikawa, J. Katoch, D. Tishler, A. M. Rao, and M. Ishigami, ACS Nano **5**, 1594 (2011).
[19]C. Cong, T. Yu, R. Saito, G. F. Dresselhaus, and M. S. Dresselhaus, ACS Nano **5**, 1600 (2011).
[20]C. Casiraghi, A. Hartschuh, H. Qian, S. Piscanec, C. Georgi, A. Fasoli, K. S. Novoselov, D. M. Basko, and A. C. Ferrari, Nano Lett. **9**, 1433 (2009).
[21]S. Ryu, M. Y. Han, J. Maultzsch, T. F. Heinz, P. Kim, M. L. Steigerwald, and L. E. Brus, Nano Lett. **8**, 4597 (2008).
[22]H. Telg, J. Maultzsch, S. Reich, F. Hennrich, and C. Thomsen, Phys. Rev. Lett. **93**, 177401 (2004).
[23]P. May, H. Telg, G. Zhong, J. Robertson, C. Thomsen, and J. Maultzsch, Phys. Rev. B **82**, 195412 (2010).
[24]C. Thomsen and S. Reich, Phys. Rev. Lett. **85**, 5214 (2000).
[25]A. C. Ferrari, J. C. Meyer, V. Scardaci, C. Casiraghi, M. Lazzeri, F. Mauri, S. Piscanec, D. Jiang, K. S. Novoselov, S. Roth, and A. K. Geim, Phys. Rev. Lett. **97**, 187401 (2006).
[26]M. Mohr, J. Maultzsch, and C. Thomsen, Phys. Rev. B **82**, 201409 (2010).
[27]P. Venezuela, M. Lazzeri, and F. Mauri, Phys. Rev. B **84**, 035433 (2011).
[28]R. Narula, N. Bonini, N. Marzari, and S. Reich, Phys. Status Solidi B **248**, 2635 (2011).
[29]R. Narula, N. Bonini, N. Marzari, and S. Reich, Phys. Rev. B **85**, 115451 (2012).
[30]Y. Kawashima and G. Katagiri, Phys. Rev. B **52**, 10053 (1995).
[31]P. H. Tan, L. An, L. Q. Liu, Z. X. Guo, R. Czerw, D. L. Carroll, P. M. Ajayan, N. Zhang, and H. L. Guo, Phys. Rev. B **66**, 245410 (2002).
[32]D. L. Mafra, G. Samsonidze, L. M. Malard, D. C. Elias, J. C. Brant, F. Plentz, E. S. Alves, and M. A. Pimenta, Phys. Rev. B **76**, 233407 (2007).
[33]T. Shimada, T. Sugai, C. Fantini, M. Souza, L. Cancado, A. Jorio, M. Pimenta, R. Saito, A. Gruneis, G. Dresselhaus *et al.*, Carbon **43**, 1049 (2005).
[34]P. T. Araujo, D. L. Mafra, K. Sato, R. Saito, J. Kong, and M. S. Dresselhaus, Phys. Rev. Lett. **109**, 046801 (2012).
[35]J. Maultzsch, S. Reich, and C. Thomsen, Phys. Rev. B **70**, 155403 (2004).
[36]F. Herziger, P. May, and J. Maultzsch, Phys. Rev. B **85**, 235447 (2012).
[37]S. Piscanec, M. Lazzeri, F. Mauri, A. C. Ferrari, and J. Robertson, Phys. Rev. Lett. **93**, 185503 (2004).
[38]A. Grüneis, J. Serrano, A. Bosak, M. Lazzeri, S. L. Molodtsov, L. Wirtz, C. Attaccalite, M. Krisch, A. Rubio, F. Mauri, and T. Pichler, Phys. Rev. B **80**, 085423 (2009).